Journal of Zhejiang University-SCIENCE A (Applied Physics & Engineering) in press
www.jzus.zju.edu.cn; www.springer.com/journal/11582
E-mail: jzus_a@zju.edu.cn

Research Article

https://doi.org/10.1631/jzus.A2400503

EPDI-transfer learning method for highly accurate prediction of lithium diffusion barriers on TMD surfaces

Jian CHEN[1,2], Yao KANG[1,2], Xudong WANG[1,2], Hao HUANG[1], Man YAO[1,2]✉

[1]*School of Materials Science and Engineering, Dalian University of Technology, Dalian 116024, China*
[2]*Key Laboratory of Solidification Control and Digital Preparation Technology (Liaoning Province), Dalian University of Technology, Dalian 116024, China*

Abstract: Calculating the inter-layer ion diffusion barrier, a crucial metric for evaluating the rate performance of 2D electrode materials, is time-consuming using the transition state search approach. A novel EPDI (electrostatic potential distribution image) transfer learning method has been proposed to efficiently and accurately predict the lithium diffusion barriers on metal element-doped transition metal dichacogenide (TMD) surfaces. Through the analysis of the mean electrostatic potential (MEP) around binding sites, a positive correlation between binding energy and MEP in VIB TMDs was identified. Subsequently, transfer learning (TL) techniques were used to develop a DenseNet121-TL model for establishing a more accurate mapping between the binding energy and electrostatic potential distribution. Trained on training sets containing 33% and 50% transition state search calculation results, which save 66% and 50% of the calculation time, respectively, the model achieves accurate predictions of the saddle point binding energy with mean absolute errors (MAEs) of 0.0444 eV and 0.0287 eV on the testing set. Based on the prediction of saddle point binding energies, we obtained a diffusion minimum energy profile with an MAE of 0.0235 eV. Furthermore, by analyzing the diffusion data, we observed that the diffusion barrier was lowered by 10% on V-doped TiS_2 compared to the stoichiometric surface. Our findings are expected to provide new insights for the high-throughput calculation of ion diffusion on 2D materials.

Key words: Transition metal dichalcogenide, Deep learning, Transfer learning, Electrostatic potential, Lithium-diffusion

Unedited

1 Introduction

A vast range of 2D materials have been widely used in energy storage systems, due to their unique physical and chemical properties compared to their bulk counterparts (Shao et al., 2019; Wu and Yu, 2019; Bahari et al., 2021; Theerthagiri et al., 2021; Theerthagiri et al., 2022a; Theerthagiri et al., 2022b). To enhance the performance of 2D materials, modification engineering has been extensively explored, including element doping (Lee et al., 2021; Wang et al., 2021b; Wang et al., 2022), defect engineering (Liu et al., 2020a; Zhang et al., 2020; Liu and Fan, 2023) and surface functional group modification (Giebeler and Balach, 2021; Zhang et al., 2021). Applying these various modification methods to 2D materials can expand the scope of exploratory material research. However, conventional experimental approaches and DFT calculations cannot keep pace with the rapidly increasing demands in the study of 2D materials. Therefore, using high-throughput DFT calculations and machine learning presents an exciting opportunity for efficient screening of the 2D materials space. Machine learning has emerged as a valuable tool to aid in high-throughput DFT calculations for predicting the properties of 2D materials (Zhan et al., 2019; Das et al., 2020; Kang et al., 2021; Ryu et al., 2022). As an advanced subfield of machine learning, deep learning exhibits enhanced feature extraction capabilities compared to conventional machine learning. It has been leveraged to analyze multidimensional raw data for screening the properties of 2D materials. Some researchers have constructed new deep neural networks tailored to their research tasks (Dong et al.,

✉ Man YAO, yaoman@dlut.edu.cn

Received Oct. 24, 2024; Revision accepted Jan. 16, 2025;
Crosschecked

© Zhejiang University Press 2025

2021; Leist et al., 2022). Using existing deep neural networks or transfer learning techniques has also yielded notable advancements in predicting the properties of 2D materials (Dong et al., 2019; Masubuchi et al., 2020).

The electrochemical properties of 2D materials determine the performance of the electrode. Machine learning has been implemented to predict these properties in the search for high-performance electrode materials. First, regarding discharge capacity, Choy et al. constructed a dataset containing the reported discharge capacities of 168 doped lithium nickel-cobalt-manganese (NCM) systems and used six regression machine learning models to predict the discharge capacity (Wang et al., 2021a). Due to the limited size of the experimental dataset, the prediction accuracy of the above models is insufficient. Besides, the complexity of the electrochemical process results in intricate nonlinear relationships between electrochemical performance and various fundamental physical parameters. Consequently, the associated datasets exhibit high-dimensional characteristics, complicating the optimization of model hyperparameters (Sendek et al., 2017; Wang et al., 2017; Liu et al., 2020b). One approach to addressing the issue of small datasets is to use existing online databases. For example, based on the C2DB 2D materials database, Kabiraj et al. selected four descriptors (Haastrup et al., 2018; Kabiraj and Mahapatra, 2022) (binding energy, rms displacement, percentage of area change, and charge transfer) to evaluate lithium storage capacity, mechanical sturdiness, and interaction strength between lithium atoms and substrates. Subsequently, Crystal Graph Convolutional Neural Network and MEGNet models were developed to predict these four descriptors (Xie and Grossman, 2018; Chen et al., 2019; Kabiraj and Mahapatra, 2022). In another example, the voltage of electrodes for multivalent metal-ion batteries was accurately predicted by an interpretable deep learning model obtained through transfer learning techniques applied to the Crystal Graph Convolutional Neural Network (Zhang et al., 2022). Moreover, Chaney et al. used a clusterwise linear regression machine learning model to predict the absorption energy of lithium on Janus Mo/WXY (X,Y = S,57 Se, Te) (Chaney et al., 2021). However, the prediction of ion diffusion performance, which plays a significant role in electrode properties, has rarely been efficient for 2D materials using machine learning. The time-consuming nature of transition state search has presented a challenge in enabling high-throughput calculations of diffusion barriers.

Here, we propose a new deep learning-based method that accurately predicts the diffusion barriers of lithium ion on the surfaces of metal element-doped transition metal dichalcogenides (TMDs) using transfer learning techniques. The developed algorithm consists of three essential sections: extraction of surface electrostatic potential distribution images, prediction of the lithium binding energies on the saddle and valley points of the surface energy profile, and transformation of binding energy to the diffusion barrier. First, considering the Coulomb interaction between lithium atoms and the surface, we hypothesized that the distribution of surface electrostatic potential significantly influences the binding energy. Therefore, we obtained a batch of 1328 fragment images representing the surface electrostatic potential distribution at valley and saddle points along the lithium diffusion path. Through area integration of the fragment images, the mean electrostatic potential (MEP) was obtained and a strong positive linear relationship between MEP and binding energy for VIB TMDs was observed, thus validating our previous conjecture. Secondly, to establish a more accurate and comprehensive mapping, we used transfer learning techniques to construct a deep neural network capable of predicting the binding energy with a mean absolute error (MAE) of 0.0287 eV. Thirdly, the diffusion barriers were calculated in batches based on the difference in binding energy between the valley and saddle points. Successive diffusion barriers were then merged to obtain the minimum diffusion path energy profile according to the diffusion path. In summary, compared to traditional machine learning, the EDPI method based on the convolutional neural network model does not require the design of complex high-dimensional feature vectors. Moreover, due to the efficient extraction of potential energy surface features of surface electrostatic potential by the convolutional neural network, this method achieves a higher prediction accuracy for diffusion barriers than those reported in the literature (Ahmed et al., 2020; Chang et al., 2021; Lu et al., 2023). The algorithm

Unedited

provides new insights into predicting diffusion barriers and expands the approach of high-throughput calculation of diffusion barriers for 2D materials.

2 Results and Discussion

2.1 Mean Electrostatic Potential

To efficiently predict the lithium diffusion barrier on the surface, it is necessary to substitute the computationally time-consuming diffusion barrier with a fast-calculated physical quantity. Through the analysis of the electron localization function (ELF) of lithium absorption on metal-doped MoS_2 with various elements (Al, Fe, Cu, Cr, Co, Zn, V, Ni, Mn) , we observed that the ELF value between lithium atoms and sulfur atoms was close to 0, indicating a weak chemical interaction during lithium absorption (Fig. S1). Consequently, the strength of Li-S bonds depends on the Coulomb interaction between the lithium and sulfur atoms, while the interaction between the lithium atom and the surface is governed mainly by the electrostatic potential distribution. Hence, we aimed to use the characteristics of the electrostatic potential distribution to predict the lithium diffusion barrier.

We speculated that the electrostatic potential is related to the adsorption energy of lithium and the surface. However, adsorption energy reflects only the energy difference between the stable states and does not account for the energy gap between the transition state and the stable state. To address this issue, we calculated the binding energy of the lithium atom at the transition state to include the information about the transition state, which is similar to the adsorption energy. Moreover, we attempted to predict the lithium binding energy based on the electrostatic potential and subsequently deduce the lithium diffusion barrier. In the following section, we outline the process for identifying the appropriate electrostatic potential distribution image in detail. At the valley points (vp) of the energy profile (Fig. 1), the lithium atom interacts mainly with three sulfur atoms, while at the saddle point (sp), two sulfur atoms form bonds with each lithium atom. Consequently, we hypothesized that

Unedited

Fig. 1: The extraction process of valley points (VP) and saddle points (SP) of the surface electrostatic potential distribution. (a) The lithium diffusion path and energy profile on the surface electrostatic potential distribution of Al doped MoS_2. The valley and saddle points are marked in red; (b) the valley and saddle points on the surface electrostatic potential distribution of Al doped MoS_2.

the electrostatic potential distributions surrounding the lithium atom at the valley and saddle points have the most influence on the binding energies of the lithium atom. Therefore, the extraction of electrostatic potential images was performed based on the hexagonal unit cell of transition metal sulfides, as shown on the right side of Fig. 1a. Additionally, the diffusion barrier was calculated as the difference in binding energy between the valley and saddle points (E_{b-vp} and E_{b-sp}). The formula derivation is shown in the supplement information file.

To overcome the time-consuming nature of the transition state search calculation, our goal was to enable high-throughput computation of E_{b-sp} by establishing a mapping relationship between the surface electrostatic potential distributions and binding energies (which include all the E_{b-vp} and part of E_{b-sp}). Then, by the difference of E_{b-vp} and E_{b-sp}, the lithium diffusion barrier could be obtained. Fig. 1b shows a selection of clipped surface electrostatic potential distribution images for the supercell surface of Al doped MoS_2. Furthermore, Fig. S2 illustrates 106 calculated surface electrostatic potential distribution images for the supercell surface of metal element-doped TMDs. To accurately batch clip these images, a Python program was developed to automate the process. Ultimately, 1328 surface electrostatic potential distribution images of the valley and saddle points were obtained, and subsequently the corresponding 1328 E_{b-vp}/E_{b-sp} values for the lithium atom were calculated using first-principles calculations with the CINEB method.

Before establishing the mapping relationship, it is crucial to validate the aforementioned speculation regarding the strong correlation between the surface electrostatic potential distribution and the binding energy. To account for the Coulomb interaction between the lithium atom and the surface, the mean surface electrostatic potential (MEP) was calculated as an indicator of the interaction strength. Furthermore, we used the Pearson correlation coefficient to assess the linear relationship between MEP and Eb (E_{b-vp} and E_{b-sp}). The Pearson correlation

Unedited

Fig. 2: Correlation between E_b of lithium atoms on metal elements ((a) Al, (b) V, (c) Cr, (d) Mn, (e) Fe, (f) Co, (g) Ni, (h) Cu, (i) Zn) doped VIB-TMD surfaces and the MEP of saddle/valley points.

coefficient (R) is a numerical value ranging from -1 to 1 used to quantify the strength and direction of a linear relationship between two variables. A large absolute value of R indicates a strong linear correlation between Eb and MEP. Based on Fig. S2, we note that doping the same atom yields comparable surface electrostatic potential distributions. The Pearson correlation coefficient R(MEP, E_b) and the relationship between E_b and MEP for surfaces doped with the same atom in VIB-TMDs (MoS_2, $MoSe_2$, WS_2, WSe_2) are shown in Fig. 2. Significantly, the Pearson correlation coefficients R(MEP, E_{b-sp}) and R(MEP, E_{b-vp}) are consistently close to 0.95 and 0.90, respectively. These results indicate a robust positive linear relationship between E_b and MEP for surfaces doped with the same atom in VIB-TMDs.

Furthermore, to examine the strength of the positive linear correlation between E_b and MEP across various atom dopings, we combined the nine images from Fig. 2 into a singular image (Fig. 3a).

Unedited

Fig. 3: Variation of Eb for lithium atoms on metal elements doped VIB-TMDs surfaces with (a) MEP and (b) the product of the number of doped atom valence electrons and mean electrostatic potential of saddle/valley points.

The data points were then visually distinguished by color, reflecting the increase in the valence electron numbers of the doped atoms. Remarkably, the data points exhibit an upward shift as the number of valence electrons of the doped atoms increases, with the exception of Al and V. Therefore, the number of valence electrons was used as a coefficient to adjust MEP (Fig. 3b). Significantly, except for Al and V, the Pearson correlation coefficient R(MEP, E_b) was 0.94, indicating a robust positive linear correlation between E_b and the product of the number of valence electrons for the doped atoms and MEP. In conclusion, the electrostatic potential and binding energy show a strong linear correlation for VIB-TMD surfaces. However, in the case of IVB and VB TMD surfaces, a weak linear correlation exists between MEP and E_b. The variation of E_b with respect to MEP is shown in Fig. S3 and Fig. S4.

2.2 Transfer learning for diffusion barrier prediction

Based on the preceding discussion, the surface electrostatic potential significantly influences the strength of interaction between lithium atoms and the surface of VIB TMDs. However, describing the interaction using MEP is not comprehensive for IVB and VB TMDs. Consequently, particular characteristics of surface electrostatic potential distributions affecting interactions were not considered in IVB and VB TMDs. To accurately and comprehensively extract the features of the surface electrostatic potential distribution that describe the interaction, we attempted to use a deep neural network with robust image feature extraction capabilities to address this challenge. However, designing and training a new deep neural network model with exceptional performance for our objective would be inefficient.

The transferability of deep neural networks is evident in their architecture: the front-end network serves as a task-agnostic feature extractor, while the backend network is closely aligned with the task at

hand(Tan et al., 2018). Therefore, unlike rebuilding a deep neural network, transfer learning enhances the model's generalization ability and prediction accuracy, while also reducing the time required for parameter tuning (Yosinski et al., 2014; Tan, et al., 2018). Thus, we aimed to use transfer learning (TL) techniques to establish our model for feature extraction of surface electrostatic potential distribution images. Consequently, the dataset was first built. Since the valley point binding energy calculation is efficient, all the valley point binding energies were added to the training set. Secondly, due to the time-consuming nature of calculating saddle point binding energies, half of these were used as the training set and the remaining half as the testing set (Fig. 4a).

Unedited

Fig. 4: (a) The left image illustrates three diffusion paths with different colors on the doped surface, while the right image shows the corresponding surface electrostatic potential distribution. In this context, the saddle point binding energy indicated by the dotted arrow serves as the test set, and that represented by the solid arrow serves as the training set. (b) Proposed approach of model-based transfer learning; (c) the testing set MAE of different models.

Moreover, six established deep neural network architectures known for their robust image feature extraction capabilities were fine-tuned, namely VGG19-TL, ResNet34-TL, ResNet101-TL, ResNet152-TL, DenseNet121-TL and DenseNet169-TL. Fig. 4b shows the model structures, wherein we retained the unchanged structure of the convolutional layers and adjusted the output of the last fully connected layer to 1. Subsequently, the input was the image depicting the local surface electrostatic potential distribution, with E_b specified as the output shown in Fig. 4b. Additionally, the model parameter was initialized using the pre-trained models VGG, ResNet and DenseNet, which had been trained on the ImageNet database. We performed 5-fold cross-validation to these models for 3000 epochs in which the mean absolute error (MAE) was set as the loss function. The MAEs of the testing set for the models with the best performance are shown in Fig. 4c. Note that the lowest MAE is 0.0287 eV for DenseNet121-TL. This MAE amounts to 0.81% of the average value (3.554 eV) for the saddle point binding energies in the testing set. This indicates that when half of the saddle point binding energies are used as the training set, the remaining half can be predicted with high accuracy. Additionally, Fig. S5 presents the performance of the best-performing models (VGG19-TL, ResNet101-TL, and DenseNet121-TL) on the testing set, along with the corresponding cumulative distribution functions of absolute errors. Furthermore, from the difference of E_{b-vp} and E_{b-sp}, a Python program was developed to convert the binding energies into diffusion barriers in batches, resulting in 318 energy profiles of the diffusion path. The Zn-doped MoS_2 surface was selected to showcase the prediction performance. Fig. S6 shows the

energy profiles for the diffusion paths on the MoS_2 surface with the other metal atoms (Al, Cu, Co, Cr, Mn, Fe, Ni, V). In Fig. 5b, all possible diffusion scenarios of the lithium atom on the Zn-doped MoS_2 surface are marked as blue, red, and purple arrows, and the overlapping sections of the three paths are highlighted in black.

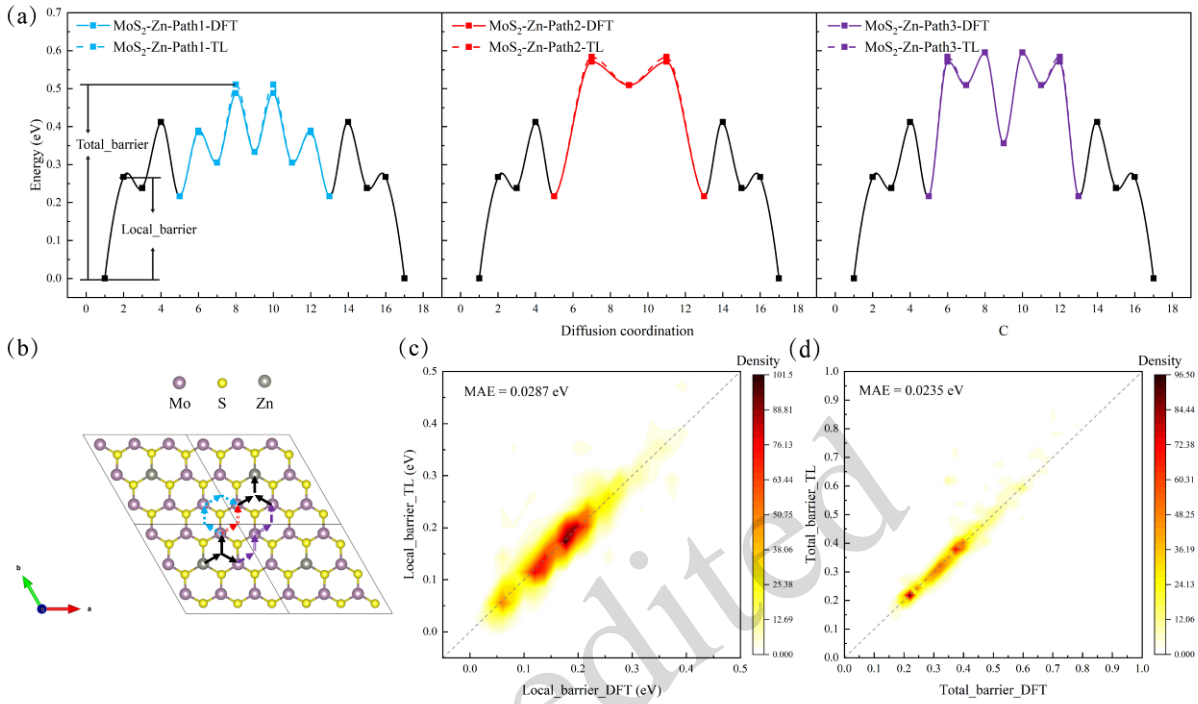

Fig. 5: Diffusion barrier prediction, (a) the DFT calculation and DenseNet121-TL prediction values of energy profile for three lithium diffusion paths on a Zn doped MoS_2 surface; (b) A schematic diagram of three lithium diffusion paths on a Zn doped MoS_2 surface; (c) The parity plot of the DFT calculation and DenseNet121-TL prediction local lithium diffusion barrier on a Zn doped MoS_2 surface; (d) The parity plot of the DFT calculation and DenseNet121-TL prediction of the total lithium diffusion barrier on a Zn doped MoS_2 surface.

Unedited

The corresponding energy profiles of these paths are shown in Fig. 5a, in which the solid lines represent the energy profiles calculated using DFT and the dotted lines depict those predicted by DenseNet121-TL. The predicted values closely align with the dotted line, indicating a high level of accuracy in the prediction of the potential barrier. Moreover, for the total metal-doped TMDs surfaces, we categorized the diffusion barriers into local and global diffusion barriers for discussion. A schematic saddle point binding energy prediction, as all valley point binding energies are calculated using DFT. Second, the model shows improved prediction performance for global diffusion barriers, achieving an MAE of 0.0235 eV. This enhancement occurs because the global diffusion barrier is influenced by the local diffusion barrier calculated using DFT (Fig. 5d).

Although the DenseNet121-TL model shows excellent prediction performance on the testing set with half of the saddle point binding energies, significant time is still required for the transition state search calculations. Therefore, we aimed to reduce the proportion of saddle point binding energies in the training set to decrease the time spent on transition state search calculations while increasing the proportion of predicted saddle point binding energies. As mentioned above, the DenseNet121-TL exhibited the best performance among the deep learning models tested. Therefore, DenseNet121-TL was chosen to train on different training sets containing 0%, 17%, and 33% proportions of saddle point binding energies. The MAE and computation time for the first-principles calculations required to prepare the training set are shown in Fig. 6. As the amount of saddle point binding energies in the training set decreases, the model's predictive performance diminishes. Besides, when the proportion of CI-NEB calculation results in the training set is 1, it indicates that

all results have been calculated using the DFT method.

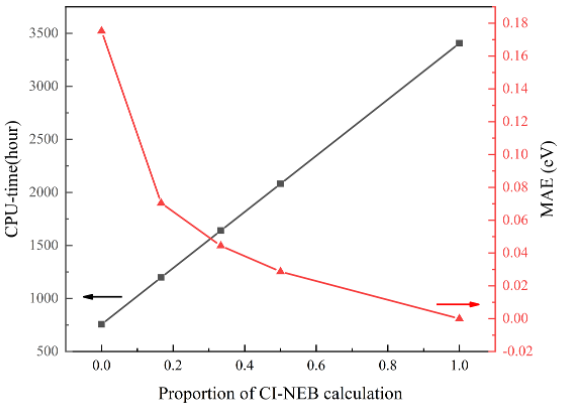

Fig. 6: The red axis shows the MAE of the DenseNet121-TL model across various training/testing sets, where all valley point binding energies and different proportions of saddle point binding energies were used as the training set, while the remaining saddle point binding energies comprised the testing set. The black axis indicates the computation time for first-principles calculations required to prepare the training set.

Therefore, for the training set containing 33% saddle point binding energies, the MAE on the testing set is 0.0444 eV, which is still excellent for diffusion barrier prediction while saving nearly 70% of the calculation time compared to the conventional DFT methods. This prediction accuracy surpasses those of the following reported machine learning methods for diffusion barrier prediction: MAE of 0.048 eV for lithium diffusion in Li_3PO_4(Li et al., 2017), MAE of 0.07/0.52 eV for copper diffusion through graphene/hBN(Ahmed, et al., 2020), and RMSE of 0.098 eV for hydrogen diffusion in alloys(Lu, et al., 2023). Furthermore, when the training set does not include saddle point binding energies, the MAE on the testing set, which contains all the saddle point binding energies, exceeds 0.16 eV, rendering it unacceptable for diffusion barrier prediction. In summary, this method requires us to provide a small number of saddle point binding energies to the model, enabling it to learn transition state information and enhance the prediction accuracy of diffusion barriers.

3 Conclusions

This paper presents a deep learning-based approach for predicting the lithium diffusion barrier on metal-doped TMD surfaces. Based on first-principles calculations, a dataset consisting of surface electrostatic potential images of valley and saddle points along the lithium diffusion path was constructed, with corresponding binding energies of lithium for metal-doped TMDs surfaces as labels. Furthermore, a strong positive correlation between the mean electrostatic potential of metal-doped VIB-TMD surfaces and the binding energies was observed. Additionally, to predict lithium diffusion barriers based on the differences in binding energies, several deep learning models were constructed using transfer learning techniques and the best model (DenseNet121-TL) was identified to establish a more accurate mapping between binding energy and electrostatic potential distribution. Trained on training sets containing 33% and 50% transition state search calculation results, the DenseNet121-TL model achieved mean absolute errors (MAEs) of 0.0444 eV and 0.0287 eV on the testing set for saddle binding energy predictions, respectively. Moreover, the lithium diffusion minimum energy profiles on metal-doped TMD surfaces were obtained with an MAE of 0.0235 eV across 106 metal-doped TMD surfaces. Furthermore, by analysis of the diffusion barrier data, the diffusion barrier was reduced by 10% on V-doped TiS_2 compared to the stoichiometric surface. Our method enables the estimation of the complete lithium diffusion minimum energy profile by requiring only a small number of transition state search calculations. We expect that our work will facilitate high-throughput calculations of lithium diffusion barriers on 2D material surfaces.

4 Methods

4.1 First-principles calculation

All density functional theory calculations in this study were performed using the projector augmented wave method (PAW)(Blöchl, 1994) implemented in the Vienna Ab initio Simulation Package (VASP)(Kresse and Furthmüller, 1996). The Perdew-Burke-Ernzerhof generalized gradient approximation (PBE-GGA)(Langreth and Mehl, 1983; Perdew et al., 1996) was used to describe the exchange-correlation energy. Van der Waals interactions were estimated using the DFT-D3 method proposed by Grimme et al. (Grimme et al., 2010). A plane wave basis set with an energy cutoff of 500 eV

Unedited

was used. The unit cell and 3×3×1 supercell configurations used 8 ×8×1 and 2×2×1 gamma central Monkhorst-Pack grids, respectively. The maximum residual force after structure relaxation was set to 0.02 eV $Å^{-1}$ for each atom, and the electronic relaxation convergence threshold was set to 10^{-5}eV. To break the periodicity in the z-direction for free surfaces, a vacuum region of 15 Å was included. To obtain the minimum energy path, the climbing image nudged elastic band (CINEB) method was used (Henkelman and Jónsson, 2000). The isosurface level for the electrostatic potential distribution on metal-doped TMD monolayer surfaces was set to 0.01 ebohr^{-3}. The lithium diffusion barriers on the stoichiometric surface of the TMDs are consistent with the findings of previous studies (Table S1). The mean electrostatic potential (MEP) is obtained by area integration using a Python program.

4.2 Dataset construction

We initially doped the monolayer surfaces of TMDs such as MoS_2, $MoSe_2$, WS_2, WSe_2, HfS_2, $HfSe_2$, TiS_2, ZrS_2, NbS_2, TaS_2, VS_2, and VSe_2 with metal heteroatoms (Al, Co, Cr, Cu, Fe, Mn, Ni, V, and Zn), resulting in a total of 106 surface configurations. Additionally, ab initio calculations were performed to determine the surface electrostatic potential distributions of 6×6×1 supercell configurations. The corresponding electrostatic potential distribution images were generated using VESTA software (Momma and Izumi, 2011) (Fig. S1). Furthermore, considering the interaction of lithium atoms with the surface at valley and saddle points along the diffusion path, a Python code was developed to extract valley point (VP) and saddle point (SP) local images from the 106 electrostatic potential distribution images, resulting in a total of 4554 images. Since the crystal exhibits periodicity and the structure around the dopant atom has central symmetry, the 4554 fragment images contain duplicates that can be obtained by rotating or flipping. After removing the duplicates, 1328 distinct fragment images were obtained, comprising 701 VP fragments and 627 SP fragments.

Subsequently, the minimum energy profiles of the lithium diffusion path for metal-doped TMD surfaces were calculated using the first-principles calculation with the CI-NEB method. Moreover, through calculation of the binding energy for a lithium atom at the valley point (marked as E_{b_VP}) and saddle points (marked as E_{b_SP}), label pairs consisting of (VP image, E_{b_VP}) and (PS image, E_{b_SP}) were established. Finally, we assigned all the label pairs of (VP image, E_{b_VP}) and different proportions (0%, 17%, 33% and 50%) of the label pairs of (PS image, E_{b_SP}) to construct the training/validation set, while the remaining label pairs of (PS image, E_{b_SP}) were allocated to the testing set to evaluate the performance of the training model.

4.3 Model and tools settings

The VGG19 (Simonyan, 2014), ResNet34/101/152(He et al., 2016), and DenseNet121/169(Huang et al., 2017) model architectures were used. These models were implemented using the PyTorch framework (Paszke et al., 2019). The outputs of these models were adjusted to one output. The weights and hyperparameters of the pre-trained models were optimized using 5-fold cross-validation, with a learning rate of 0.00005 and a total of 3000 epochs. The batch size of the training, validation, and testing sets were set to 40, 16 and 16, respectively. Data augmentation techniques were used to generate additional training data and enhance the generalization capability of the model.

Uncorrected

Acknowledgments

This work is supported by the National Natural Science Foundation of China (Nos. 51974056 and 51474047), the Supercomputing Center of Dalian University of Technology, and the Key Laboratory of Solidification Control and Digital Preparation Technology (Liaoning Province)..

Author contributions

Jian Chen performed all the first-principles calculations, developed the algorithms based on the deep learning model and wrote the manuscript. Yao Kang contributed to establishment of the datasets. Xudong Wang and Hao Huang helped with developing ideas. Man Yao helped with writing and data analysis.

Conflict of interest

Jian Chen, Yao Kang, Xudong Wang, Hao Huang, Man Yao declare that they have no conflict of interest.

References

Ahmed M, Li Y, Chen W, et al., 2020. Diffusion barrier prediction of graphene and boron nitride for copper interconnects by deep learning. *IEEE Access*, 8:210542-210549. https://doi.org/10.1109/ACCESS.2020.3039257

Bahari Y, Mortazavi B, Rajabpour A, et al., 2021. Application of two-dimensional materials as anodes for rechargeable metal-ion batteries: A comprehensive perspective from density functional theory simulations. *Energy Storage Materials*, 35:203-282. https://doi.org/10.1016/j.ensm.2020.11.004

Blöchl PE, 1994. Projector augmented-wave method. *Physical Review B*, 50(24):17953-17979. https://doi.org/10.1103/PhysRevB.50.17953

Chaney G, Ibrahim A, Ersan F, et al., 2021. Comprehensive study of lithium adsorption and diffusion on janus mo/wxy (x, y = s, se, te) using first-principles and machine learning approaches. *ACS Applied Materials & Interfaces*, 13(30):36388-36406. https://doi.org/10.1021/acsami.1c05508

Chang JH, Jørgensen PB, Loftager S, et al., 2021. On-the-fly assessment of diffusion barriers of disordered transition metal oxyfluorides using local descriptors. *Electrochimica Acta*, 388:138551. https://doi.org/10.1016/j.electacta.2021.138551

Chen C, Ye W, Zuo Y, et al., 2019. Graph networks as a universal machine learning framework for molecules and crystals. *Chemistry of Materials*, 31(9):3564-3572. https://doi.org/10.1021/acs.chemmater.9b01294

Das S, Pegu H, Sahu KK, et al., 2020. 19 - machine learning in materials modeling—fundamentals and the opportunities in 2d materials. In: Yang, E.-H., Datta, D., Ding, J., et al. Eds.), Synthesis, modeling, and characterization of 2d materials, and their heterostructures. Elsevier, p.445-468.

Dong X, Li H, Jiang Z, et al., 2021. 3d deep learning enables accurate layer mapping of 2d materials. *ACS Nano*, 15(2):3139-3151. https://doi.org/10.1021/acsnano.0c09685

Dong Y, Wu C, Zhang C, et al., 2019. Bandgap prediction by deep learning in configurationally hybridized graphene and boron nitride. *npj Computational Materials*, 5(1):26. https://doi.org/10.1038/s41524-019-0165-4

Giebeler L, Balach J, 2021. Mxenes in lithium–sulfur batteries: Scratching the surface of a complex 2d material – a minireview. *Materials Today Communications*, 27:102323. https://doi.org/10.1016/j.mtcomm.2021.102323

Grimme S, Antony J, Ehrlich S, et al., 2010. A consistent and accurate ab initio parametrization of density functional dispersion correction (dft-d) for the 94 elements h-pu. *The Journal of Chemical Physics*, 132(15):154104. https://doi.org/10.1063/1.3382344

Haastrup S, Strange M, Pandey M, et al., 2018. The computational 2d materials database: High-throughput modeling and discovery of atomically thin crystals. *2D Materials*, 5(4):042002. https://doi.org/10.1088/2053-1583/aacfc1

He, K, Zhang, X, Ren, S, et al., 2016. Deep residual learning for image recognition. In Proceedings of the IEEE conference on computer vision and pattern recognition, p. 770-778. https://openaccess.thecvf.com/content_cvpr_2016/html/He_Deep_Residual_Learning_CVPR_2016_paper.html

Henkelman G, Jónsson H, 2000. Improved tangent estimate in the nudged elastic band method for finding minimum energy paths and saddle points. *The Journal of Chemical Physics*, 113(22):9978-9985. https://doi.org/10.1063/1.1323224

Huang, G, Liu, Z, Van Der Maaten, L, et al., 2017. Densely connected convolutional networks. In Proceedings of the IEEE conference on computer vision and pattern recognition, p. 4700-4708. https://openaccess.thecvf.com/content_cvpr_2017/html/Huang_Densely_Connected_Convolutional_CVPR_2017_paper.html

Kabiraj A, Mahapatra S, 2022. High-throughput assessment of two-dimensional electrode materials for energy storage devices. *Cell Reports Physical Science*, 3(1) https://doi.org/10.1016/j.xcrp.2021.100718

Kang Y, Li L, Li B, 2021. Recent progress on discovery and properties prediction of energy materials: Simple machine learning meets complex quantum chemistry. *Journal of Energy Chemistry*, 54:72-88. https://doi.org/10.1016/j.jechem.2020.05.044

Kresse G, Furthmüller J, 1996. Efficient iterative schemes for ab initio total-energy calculations using a plane-wave basis set. *Physical Review B*, 54(16):11169-11186. https://doi.org/10.1103/PhysRevB.54.11169

Langreth DC, Mehl MJ, 1983. Beyond the local-density approximation in calculations of ground-state electronic properties. *Physical Review B*, 28(4):1809-1834. https://doi.org/10.1103/PhysRevB.28.1809

Lee SJ, Theerthagiri J, Nithyadharseni P, et al., 2021. Heteroatom-doped graphene-based materials for sustainable energy applications: A review. *Renewable and Sustainable Energy Reviews*, 143:110849. https://doi.org/10.1016/j.rser.2021.110849

Leist C, He M, Liu X, et al., 2022. Deep-learning pipeline for statistical quantification of amorphous two-dimensional materials. *ACS Nano*, 16(12):20488-20496. https://doi.org/10.1021/acsnano.2c06807

Li W, Ando Y, Minamitani E, et al., 2017. Study of li atom diffusion in amorphous li3po4 with neural network potential. *The Journal of Chemical Physics*, 147(21):214106. https://doi.org/10.1063/1.4997242

Liu F, Fan Z, 2023. Defect engineering of two-dimensional materials for advanced energy conversion and storage. *Chemical Society Reviews*, 52(5):1723-1772. https://doi.org/10.1039/D2CS00931E

Liu H, Lei W, Tong Z, et al., 2020a. Defect engineering of 2d materials for electrochemical energy storage. *Advanced Materials Interfaces*, 7(15):2000494. https://doi.org/10.1002/admi.202000494

Liu Y, Wu J-M, Avdeev M, et al., 2020b. Multi-layer feature selection incorporating weighted score-based expert knowledge toward modeling materials with targeted properties. *Advanced Theory and Simulations*,

Unedited

3(2):1900215. https://doi.org/10.1002/adts.201900215

Lu GM, Witman M, Agarwal S, et al., 2023. Explainable machine learning for hydrogen diffusion in metals and random binary alloys. *Physical Review Materials*, 7(10):105402. https://doi.org/10.1103/PhysRevMaterials.7.105402

Masubuchi S, Watanabe E, Seo Y, et al., 2020. Deep-learning-based image segmentation integrated with optical microscopy for automatically searching for two-dimensional materials. *npj 2D Materials and Applications*, 4(1):3. https://doi.org/10.1038/s41699-020-0137-z

Momma K, Izumi F, 2011. Vesta 3 for three-dimensional visualization of crystal, volumetric and morphology data. *Journal of Applied Crystallography*, 44(6):1272-1276. https://doi.org/10.1107/S0021889811038970

Paszke A, Gross S, Massa F, et al., 2019. Pytorch: An imperative style, high-performance deep learning library. *Advances in neural information processing systems*, 32

Perdew JP, Burke K, Ernzerhof M, 1996. Generalized gradient approximation made simple. *Physical Review Letters*, 77(18):3865-3868. https://doi.org/10.1103/PhysRevLett.77.3865

Ryu B, Wang L, Pu H, et al., 2022. Understanding, discovery, and synthesis of 2d materials enabled by machine learning. *Chemical Society Reviews*, 51(6):1899-1925. https://doi.org/10.1039/D1CS00503K

Sendek AD, Yang Q, Cubuk ED, et al., 2017. Holistic computational structure screening of more than 12 000 candidates for solid lithium-ion conductor materials. *Energy & Environmental Science*, 10(1):306-320. https://doi.org/10.1039/C6EE02697D

Shao Q, Wu Z-S, Chen J, 2019. Two-dimensional materials for advanced li-s batteries. *Energy Storage Materials*, 22:284-310. https://doi.org/10.1016/j.ensm.2019.02.001

Simonyan K, 2014. Very deep convolutional networks for large-scale image recognition. *arXiv preprint arXiv:1409.1556*,

Tan, C, Sun, F, Kong, T, et al., 2018. A survey on deep transfer learning. In Artificial Neural Networks and Machine Learning–ICANN 2018: 27th International Conference on Artificial Neural Networks, Rhodes, Greece, October 4-7, 2018, Proceedings, Part III 27 p. 270-279. Springer International Publishing.
https://doi.org/10.1007/978-3-030-01424-7_27

Theerthagiri J, Lee Seung j, Karuppasamy K, et al., 2021. Application of advanced materials in sonophotocatalytic processes for the remediation of environmental pollutants. *Journal of Hazardous Materials*, 412:125245. https://doi.org/10.1016/j.jhazmat.2021.125245

Theerthagiri J, Karuppasamy K, Lee SJ, et al., 2022a. Fundamentals and comprehensive insights on pulsed laser synthesis of advanced materials for diverse photo- and electrocatalytic applications. *Light: Science & Applications*, 11(1):250. https://doi.org/10.1038/s41377-022-00904-7

Theerthagiri J, Park J, Das HT, et al., 2022b. Electrocatalytic conversion of nitrate waste into ammonia: A review. *Environmental Chemistry Letters*, 20(5):2929-2949. https://doi.org/10.1007/s10311-022-01469-y

Wang G, Fearn T, Wang T, et al., 2021a. Machine-learning approach for predicting the discharging capacities of doped lithium nickel–cobalt–manganese cathode materials in li-ion batteries. *ACS Central Science*, 7(9):1551-1560. https://doi.org/10.1021/acscentsci.1c00611

Wang R, Li M, Sun K, et al., 2022. Element-doped mxenes: Mechanism, synthesis, and applications. *Small*, 18(25):2201740. https://doi.org/10.1002/smll.202201740

Wang X, Xiao R, Li H, et al., 2017. Quantitative structure-property relationship study of cathode volume changes in lithium ion batteries using ab-initio and partial least squares analysis. *Journal of Materiomics*, 3(3):178-183. https://doi.org/10.1016/j.jmat.2017.02.002

Wang X, Meng L, Li B, et al., 2021b. Heteroatoms/molecules to tune the properties of 2d materials. *Materials Today*, 47:108-130. https://doi.org/10.1016/j.mattod.2020.12.019

Wu Y, Yu Y, 2019. 2d material as anode for sodium ion batteries: Recent progress and perspectives. *Energy Storage Materials*, 16:323-343. https://doi.org/10.1016/j.ensm.2018.05.026

Xie T, Grossman JC, 2018. Crystal graph convolutional neural networks for an accurate and interpretable prediction of material properties. *Physical Review Letters*, 120(14):145301. https://doi.org/10.1103/PhysRevLett.120.145301

Yosinski J, Clune J, Bengio Y, et al., 2014. How transferable are features in deep neural networks? *Advances in neural information processing systems*, 27

Zhan C, Sun W, Xie Y, et al., 2019. Computational discovery and design of mxenes for energy applications: Status, successes, and opportunities. *ACS Applied Materials & Interfaces*, 11(28):24885-24905. https://doi.org/10.1021/acsami.9b00439

Zhang W, Liu S, Chen J, et al., 2021. Exploring the potentials of ti3cin2–itx (i = 0, 1, 2)-mxene for anode materials of high-performance sodium-ion batteries. *ACS Applied Materials & Interfaces*, 13(19):22341-22350. https://doi.org/10.1021/acsami.1c02470

Zhang X, Zhou J, Lu J, et al., 2022. Interpretable learning of voltage for electrode design of multivalent metal-ion batteries. *npj Computational Materials*, 8(1):175. https://doi.org/10.1038/s41524-022-00858-9

Zhang Y, Tao L, Xie C, et al., 2020. Defect engineering on electrode materials for rechargeable batteries. *Advanced Materials*, 32(7):1905923. https://doi.org/10.1002/adma.201905923

中文概要

Unedited

题　目：基于 EPDI-迁移学习的 TMD 表面锂扩散势垒高精度预测方法

作　者：陈健[1,2]，康瑶[1,2]，王旭东[1,2]，黄昊[1]，姚曼[1,2]

机　构：[1]大连理工大学，材料科学与工程学院，中国大连，116024；[2]大连理工大学，辽宁省凝固控制与数字化制备技术重点实验室，中国大连，116024.

目　的：表面锂扩散势垒是评价二维电极材料倍率性能的关键参数之一。基于过渡态搜索的扩散势垒计算方法是一种广泛使用但计算耗时的方法。本文以金属元素掺杂的二维过渡金属硫化物为研究对象，旨在借助卷积神经网络和迁移学习技术构建局部表面静电势分布图像与锂结合能的映射关系，以此实现表面锂扩散势能曲线的高效准确预测。

创新点：基于卷积神经网络的可迁移性，借助用于图像识别的深度学习模型，构建了局部表面静电势分布图像与锂结合能的映射关系，并以此实现了锂扩散路径上势能曲线的高效预测。

方　法：1. 通过基于密度泛函理论的第一性原理计算，揭示了金属元素掺杂VIB族过渡金属硫化物表面的局部静电势均值与锂结合能的强正相关性；2. 针对金属元素掺杂 IVB,VB 和 VIB 族过渡金属硫化物，构建局部静电势图像及锂结合能数据库，借助迁移学习方法搭建多种深度学习模型，调参优化训练模型，对比训练后不同模型预测效果的差异性；3. 选取最优模型，调节训练集中过渡态计算数据的数量，预测不同锂扩散路径上的势能曲线，对比过渡态搜索方法，证明了 EPDI-迁移学习方法的高预测精度和低耗时性。

结　论：1.金属元素掺杂 VIB 族过渡金属硫化物表面的局部静电势均值与锂结合能呈现强正相关性；2. 借助迁移学习技术的 DenseNet121-TL 模型能够实现鞍点结合能的准确预测，当训练集包含 33%的鞍点结合能数据时，对其余鞍点结合能的平均绝对预测误差为 0.0444eV；3. 利用对鞍点结合能的预测实现了锂扩散路径上势能曲线的高效预测。

关键词：过渡金属硫族化物；深度学习；迁移学习；静电势；锂扩散

Unedited